

AD-A051 193

HARRY DIAMOND LABS ADELPHI MD

F/G 20/14

EMP SCALE-MODEL TESTING OF AN ARMY BRIGADE SIGNAL CENTER.(U)

DEC 77 A A CUNEO, J J LOFTUS, R A DYCKSON

UNCLASSIFIED

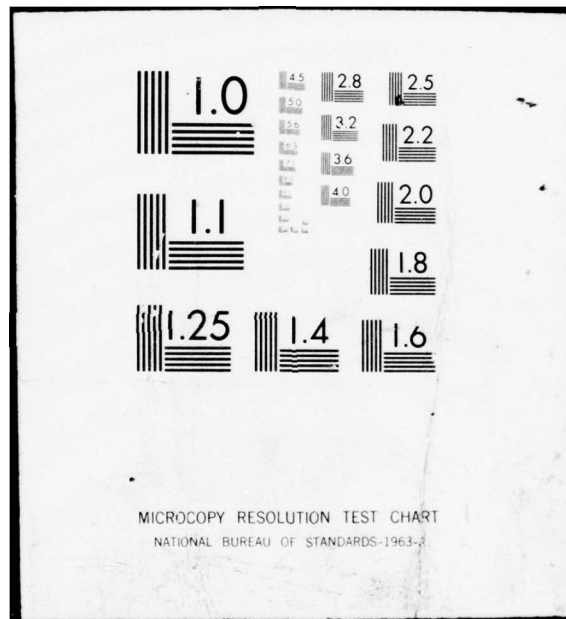
HDL-TM-77-29

NL

| OF |

AD
A051 193





HDL-TM-77-29

12

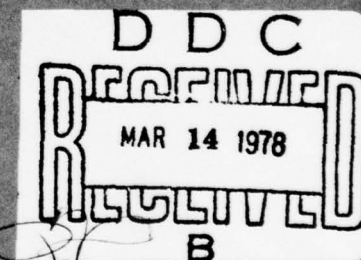
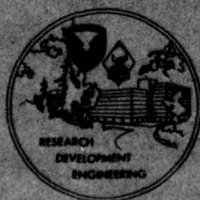
AD A051193

EMP Scale-Model Testing of an Army Brigade Signal Center

December 1977

HDL-TM-77-29—EMP Scale-Model Testing of an Army Brigade Signal Center,
by Andrew A. Cuneo, Jr., James J. Loftus, and Robert A. Dyckson

AD No. _____
DDC FILE COPY



U.S. Army Materiel Development
and Readiness Command
HARRY DIAMOND LABORATORIES
Adelphi, Maryland 20783

The findings in this report are not to be construed as an official Department of the Army position unless so designated by other authorized documents.

Citation of manufacturers' or trade names does not constitute an official indorsement or approval of the use thereof.

Destroy this report when it is no longer needed. Do not return it to the originator.

UNCLASSIFIED
SECURITY CLASSIFICATION OF THIS PAGE (When Data Entered)

REPORT DOCUMENTATION PAGE		READ INSTRUCTIONS BEFORE COMPLETING FORM
1. REPORT NUMBER HDL-TM-77-29	2. GOVT ACCESSION NO.	3. RECIPIENT'S CATALOG NUMBER
4. TITLE (and Subtitle) EMP Scale-Model Testing of an Army Brigade Signal Center.	5. TYPE OF REPORT & PERIOD COVERED Technical Memo	6. PERFORMING ORG. REPORT NUMBER
7. AUTHOR(s) Andrew A./Cuneo, Jr., James J./Loftus Robert A./Dyckson	8. CONTRACT OR GRANT NUMBER(s) DA: 1W162118AH75 PRON: A16R000401A1A9	
9. PERFORMING ORGANIZATION NAME AND ADDRESS Harry Diamond Laboratories 2800 Powder Mill Road Adelphi, MD 20783	10. PROGRAM ELEMENT, PROJECT, TASK AREA & WORK UNIT NUMBERS Program Ele: 6.21.18.A	
11. CONTROLLING OFFICE NAME AND ADDRESS US Army Materiel Development and Readiness Command Alexandria, VA 22333	12. REPORT DATE December 1977	13. NUMBER OF PAGES 38p.
14. MONITORING AGENCY NAME & ADDRESS (if different from Controlling Office)	15. SECURITY CLASS. (of this report) UNCLASSIFIED	15a. DECLASSIFICATION/DOWNGRADING SCHEDULE
16. DISTRIBUTION STATEMENT (of this Report) Approved for public release; distribution unlimited.		
17. DISTRIBUTION STATEMENT (of the abstract entered in Block 20, if different from Report)		
18. SUPPLEMENTARY NOTES HDL Project: X756E4 DRCMS Code: 612118.H750011 This project was sponsored under the Multiple Systems Evaluation Program.		
19. KEY WORDS (Continue on reverse side if necessary and identify by block number) EMP Incident Scale model Angles Brigade Azimuth		
20. ABSTRACT (Continue on reverse side if necessary and identify by block number) An EMP (electromagnetic pulse) simulation test is conducted on a U.S. Army brigade signal center in 1/100 scale. The bulk currents induced on the modeled system are recorded as the azimuth and angle of incidence of the model simulator are varied. Plots are presented of the peak amplitude of the current versus azimuth angle for various angles of elevation. A compari-		

DD FORM 1 JAN 73 1473 EDITION OF 1 NOV 65 IS OBSOLETE

UNCLASSIFIED

1 SECURITY CLASSIFICATION OF THIS PAGE (When Data Entered)

DDC
RECEIVED
MAR 14 1978
B

163 050

IL

UNCLASSIFIED

SECURITY CLASSIFICATION OF THIS PAGE(When Data Entered)

son is made between the response of the system and that of a single long cable buried near the surface of the ground.



ACCESSION for	
NTIS	White Section <input checked="" type="checkbox"/>
DDC	Buff Section <input type="checkbox"/>
UNANNOUNCED	<input type="checkbox"/>
JUSTIFICATION	
BY	
DISTRIBUTION/AVAILABILITY CODES	
Dist. AVAIL. and/or SPECIAL	
A	

UNCLASSIFIED

SECURITY CLASSIFICATION OF THIS PAGE(When Data Entered)

CONTENTS

	<u>Page</u>
1. INTRODUCTION	5
2. BRIGADE SIGNAL CENTER DESCRIPTION	5
3. MODELING	6
3.1 Theory	6
3.2 Application	7
3.3 Scale-Modeling Facility	8
4. INSTRUMENTATION	9
4.1 Pulse Generator	9
4.2 Pulse Radiator	9
4.3 Measurement Equipment	10
5. EXPERIMENTAL DATA	11
5.1 Approach	11
5.2 Analysis	14
6. CONCLUSIONS	25
LITERATURE CITED	26
APPENDIX A.--ADDITIONAL BSC INFORMATION	27
DISTRIBUTION	29

FIGURES

1 Scale modeling facility	8
2 Loaded dipole illuminator	10
3 Brigade signal center	11
4 BSC model looking directly at AN/TRC-145	12
5 BSC model viewed broadside	12
6 Azimuthal layout of BSC and illuminator	13
7 Waveforms as function of angle of incidence	14
8 Waveforms as function of azimuth angle	15
9 Absolute peak amplitude versus azimuth angle	16

FIGURES (Cont'd)

	<u>Page</u>
10 First peak amplitude versus azimuth angle	18
11 Absolute peak plot	21
12 First peak plot	22
13 Variation of peak cable current as azimuth (ϕ) and elevation (ψ) angles of incidence change	24

TABLES

I	Peak Current Values as Function of Azimuth Angle for Constant Angle of Incidence	17
II	Slope Change Amplitude Point	19
III	Absolute Peak Value Normalized to $\beta = 90$ deg, $\phi = 90$ deg .	23
IV	First Peak (Slope Change) Value Normalized to $\beta = 90$ deg, $\phi = 90$ deg	23

1. INTRODUCTION

The electromagnetic pulse (EMP) accompanying the detonation of a nuclear weapon at high altitudes can extend over several thousand square miles and cause severe damage to military electronic equipment. Potentially vulnerable are communications complexes covering large areas linked together by field wires. These wires provide excellent means for coupling large amounts of energy from the incident field into the electronics.

The Harry Diamond Laboratories (HDL) performed EMP testing of a scale model of a U.S. Army brigade signal center (BSC). The approach taken in testing this forward field-area communications complex was similar in part to "real world" EMP testing, in that a pulse with very fast risetime and relatively slow fall time was used to illuminate the scaled system, and the induced bulk currents were observed and recorded. Markedly different, however, was the way that the system was illuminated.

In the "real world" EMP testing of communication systems composed of many widely separated components, attempts to test the entire system at once are confronted with several serious constraints. In using a fixed-position simulator, the choice of angles of incidence and azimuth of the arriving simulated EMP are generally limited by the chosen field strength and physical limitations on the layout of the simulator. In this test, the response of the BSC model was observed from every azimuthal angle at four angles of incidence.

This work was initiated in support of the Army's Multiple Systems Evaluation Program (MSEP) to serve as a guide in the analysis of the BSC.

2. BRIGADE SIGNAL CENTER DESCRIPTION

The mission of the Army signal brigade¹⁻³ requires that its assigned signal units provide both command and area signal communications 24 hours a day. Accordingly, elements of the brigade staff must operate in a like manner--particularly the systems control and operations section, which is actively engaged in maintaining control over operation of the BSC. However, techniques used to execute the operation may vary with particular tactical situations within the Army.

¹U.S. Army FM 11-125, *Field Army Signal Communications*, Headquarters Dept. Army (December 1969).

²U.S. Army FM 24-16, *Signal Orders Records and Reports*, Headquarters Dept. Army (May 1970).

³U.S. Army FM 24-18, *Field Radio Techniques*, Headquarters Dept Army (July 1965).

The BSC is the forward portion of a field-Army communications complex. It is linked with the main echelons by way of multichannel radio, radio Teletype, and/or cable. The main echelon consists of division, corps, and army. It is tied in to the front echelons by way of FM-voice radio, telephone switchboards, and multichannel radio. The front consists of battalions, companies, platoons, squadrons, and special forces teams using hf-voice cw radio. Wire communications are employed primarily between the brigade commander, staff members, and attached and supporting units in the brigade base. The distance between headquarters and subordinate units, rapidly changing situations, limited wire construction personnel, and equipment in the brigade will generally preclude elaborate wire trunking systems. The characteristics of the area of operations have a great influence on communications planning. These characteristics include weather, terrain, size, and shape of the area of operations.

Most communications equipment used in the BSC is vehicular: vans, shelters, etc. A description of some of the equipment, its placement, and its general setup is found in appendix A.

The scale model of the BSC was set up with a minimum of vehicles and other equipment; however, these items were placed like a setup which might very well be used in the field. The BSC is not a fixed type of organization. The size and composition may vary in different areas. Other signal units (separate companies and teams) may be assigned or attached to augment its capabilities or to perform special signal functions.

An advantage of a scale-model test is that other equipment may be easily included in the system at any given time to observe EMP response changes.

3. MODELING

3.1 Theory

The fact that electromagnetic scale modeling is possible in general is due to the linearity of Maxwell's equations which describe the fields in any electromagnetic system. It is necessary therefore to eliminate nonlinear media from the system of interest. In theory, it is not necessary to exclude nonhomogeneous media, since Maxwell's equations are valid for nonhomogeneous as well as homogeneous media.

Sinclair⁴ shows that "for an arbitrary choice of the four scale factors p , α , β and γ it is theoretically possible to construct an exact model to simulate a given full-scale system." The scale factors are defined as follows.

p = mechanical scale factor

α = scale factor for electrical intensity

β = scale factor for magnetic intensity

γ = scale factor for time

Sinclair proceeds to show that when air in the full-scale system is simulated with air in the model, the following relationships are established for all media being modeled:

$\mu' = \mu$ (permeability)

$\epsilon' = \epsilon$ (permittivity)

$\sigma' = p\sigma$ (conductivity)

$p = \gamma$

$\alpha = \beta$

where the primed macroscopic properties refer to the model media and the unprimed properties refer to the full-scale system.

3.2 Application

For the BSC model, $p = 100$, so that all physical dimensions have been scaled down by $\sim 1/100$. Copper was used to fabricate all shelters, trucks, and cables, because copper affords the highest practical value of conductivity. Kreck⁵ has shown that the wire resistivity ($1/\text{conductivity}$) and diameter used in the model can vary over a range of values without seriously altering the current. In addition, the dominant loss mechanism for wires lying on the ground is the soil conductivity. Consequently, the failure to scale the system-cable conductivity does not appear to be a real problem. The soil conductivity of the model was $\sigma' \sim 0.2$ mho/m.

⁴G. Sinclair, *Theory of Models of Electromagnetic Systems*, Proc. Institute of Radio Engineers (November 1948), 1364-1370.

⁵J. Kreck, *Electromagnetic Scale Model of TEMPS/Polk City Test Configuration*, Harry Diamond Laboratories TR-1717 (March 1976).

Previous tests at this facility have shown that the risetime of the currents induced in buried cables increases significantly as compared to the radiated-field risetime because of the high frequency losses in the ground. These losses will also increase the risetime for wires lying on the ground as in the case of the BSC. This increase is of practical value in that truly scaling (1/100) the risetime of a simulated EMP was beyond the capability of the model simulators. Actual EMP field simulators can currently radiate fields with risetimes of between 5 and 10 ns. True 1/100 scaling of this parameter would require a field with a risetime of between 50 and 100 ps. As will be seen in the next section, the model field risetime had a value of ~250 ps.

3.3 Scale-Modeling Facility

The HDL Electromagnetic Scale Modeling Facility occupies a large essentially wooden structure at the North Annex of Fort Belvoir. The structure, which is known as the "FREME" (Facility for Research in Electromagnetic Effects), is approximately 46×30 m with the highest point of the roof 15 m above the floor.

The modeling is carried out in an 18×24 m box containing chemically treated sand of 10 cm average depth. The recording instrumentation is on the level below the sand box (see fig. 1, showing the interior of the FREME).

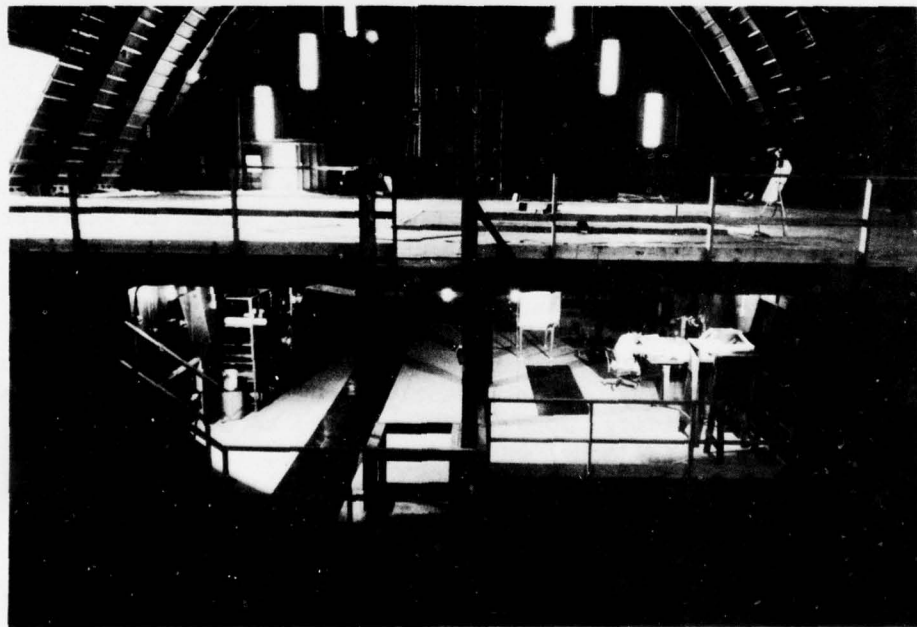


Figure 1. Scale-modeling facility.

112-73E

4. INSTRUMENTATION

4.1 Pulse Generator

The pulse generator used for this test was designed and built by HDL personnel. It consists of a coaxial-cable charge line of variable length attached to a commercial high-voltage dc power supply. This discharges through the contacts of a mercury-wetted reed relay to the attached load. The mercury switch is housed in an aluminum casing which closely maintains a 50-ohm coaxial configuration from the charge line to the load. The aluminum allows the switch to be repetitively operated by the field induced from an ac-line-fed coil surrounding the casing. The output of this device is a variable-length pulse with a risetime ≤ 150 ps and a level of up to 1000 V into 50 ohms. The shape of the pulse is determined by a series capacitor inserted in the output. The output pulse is then coupled to the model antenna through a low-loss coaxial line.

4.2 Pulse Radiator

The pulse output of the generator was used to illuminate the BSC model through an antenna called a loaded dipole (LDP). The LDP antenna is a cylindrical dipole which is center fed by a bicone (fig. 2). This bicone has a half angle of approximately 7 deg, yielding an impedance of 300 ohms, and a half length of 0.46 m, which is easily sufficient to launch the leading edge of the pulse without distortion. The bicone is joined to two 10-cm-diam cylinders which radiate the late time of the pulse. The overall length of the LDP is 6.6 m.

One side of the LDP is at dc ground and is used to house the rf coaxial cable which conducts the remotely generated pulse to the bicone apex. The other side of the antenna is connected to the center conductor of the coaxial cable. End reflections are minimized by loading the ends of the antenna with rf-absorbent material.

The output of the generator was adjusted to yield a 640-V pulse applied to the LDP bicone, which, with an impedance-mismatch factor* of 1.7, provided a bicone voltage of 1080 V. At a distance of 3 m, in the equatorial plane of the bicone, the calculated value of the free electric field is 72 V/m. The radiated output of the LDP was observed by a differential electric-field probe and by a current transformer across a slot in an artificial ground plane.⁶ These observations show the electric field risetime to be 250 ps (10 to 90 percent) and the magnetic-field pulse length (or time to crossover) to be 18 ns.

⁶A. Cuneo and J. Loftus, *Scale Modeling for the PAR EMP Test*, Harry Diamond Laboratories TR-1761 (September 1976).

*The voltage reflection coefficient is 0.7.

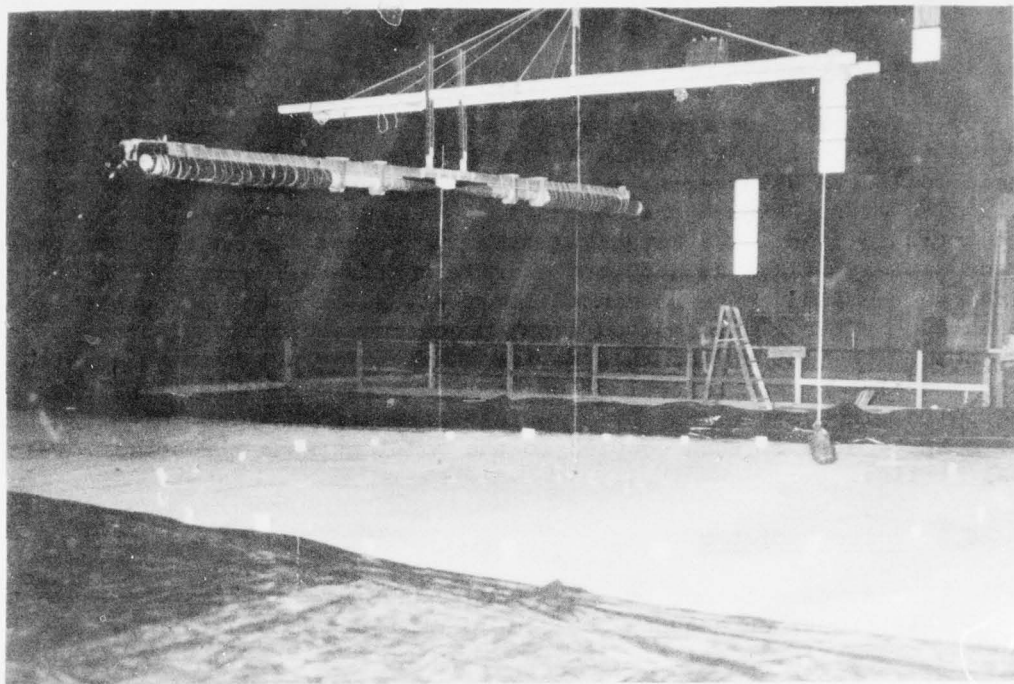


Figure 2. Loaded dipole (LDP) illuminator.

117-76

4.3 Measurement Equipment

The data for this test were recorded in oscillograph form from the following real-time measurement equipment:

- Tektronix C51 oscilloscope camera
- Tektronix type 7904 oscilloscope
- Tektronix type 7B92 time-base
- Tektronix type 7A19 vertical amplifiers (risetime $t_r \leq 800$ ps)
- Tektronix type CT-1 current transformers ($t_r \leq 350$ ps)

On those occasions in the preliminary testing when the risetime of an observed waveform appeared to be approaching the specification limit of this system, Tektronix type 7S11 sampling units with S-6 sampling heads and a type 7T11 sampling sweep unit were substituted in the 7904 oscilloscope mainframe. The fastest risetime observed under these conditions was 0.8 ns (10 to 90 percent), which occurred only once. It was discernible at all other times that the risetimes of the waveforms were within the real-time equipment specification.

5. EXPERIMENTAL DATA

5.1 Approach

The BSC described in section 2 was constructed in model form, scaled down in size by a factor of 100. The model (fig. 3) was arranged in a field-deployment configuration on the chemically treated sand of the test area (fig. 4, 5), and grounded as in the real world at every vehicle and the switchboard. As in previous tests at this facility,⁶ the model was subjected to simulated EMP through the use of the LDP antenna described in section 4.2. A device (fig. 2) was constructed for this project which allowed the LDP to be rotated in azimuth (ϕ) and varied in elevation (β)* with respect to the modeled BSC. This device provided the means for the collection of a great deal of informative data. The ladder-like structure was suspended above the test volume by a rope and pulley arrangement which was operated by two remote electric winches. The LDP was attached and positioned so that the entire apparatus could be rotated in azimuth around one fixed point in the test volume.

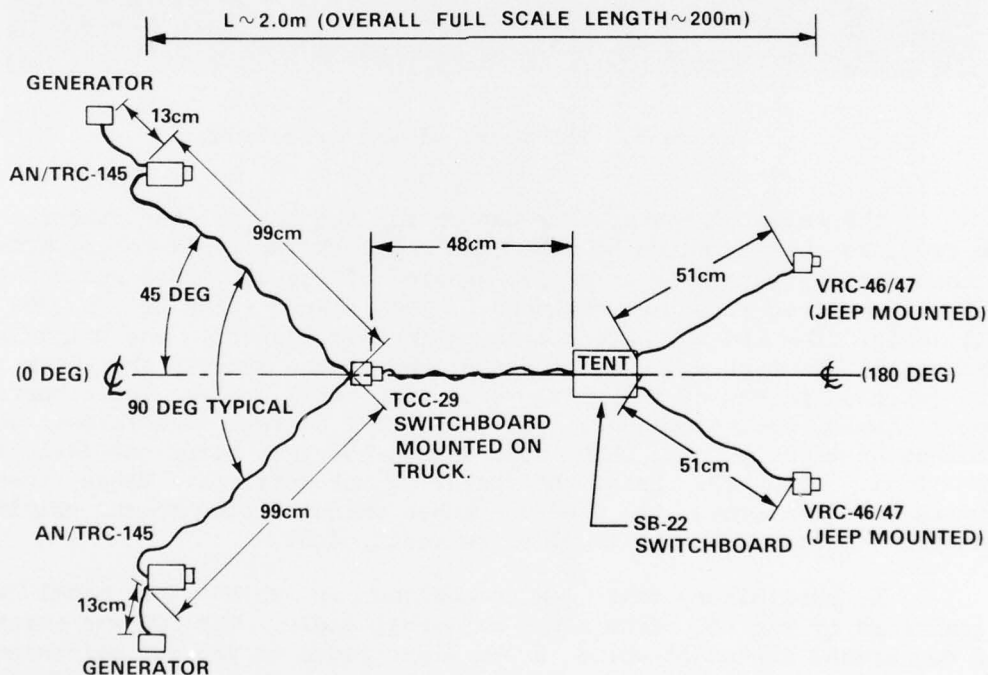


Figure 3. Brigade signal center (all hard-wire connections).

⁶A. Cuneo and J. Loftus, *Scale Modeling for the PAR EMP Test*, Harry Diamond Laboratories TR-1761 (September 1976).

* β measures the angle between the vector joining the center of the antenna to the center of rotation (in BSC) and the ground.



Figure 4. BSC model looking directly at AN/TRC-145. 114-76



Figure 5. BSC model viewed broadside. 115-76

The selected center of rotation for the LDP was the junction of the two long wires which couple the model AN/TRC-145's to the TCC-29 switchboard. Figure 6 is a scale drawing of the BSC model and the LDP with the rotating structure excluded. The slant range of 3 m (300 m, full scale) from the LDP bicone apex to the wire junction was maintained throughout this test. The model was placed on the sand so that both the wire junction points of the model were over small holes where current probes could be implemented. Textronix CT-1 current transformers were attached at these points, which were designated test point one (TP1) and two (TP2), with TP1 being the center of LDP rotation. These transformers were attached to P-6040 probes which coupled to the shielded equipment enclosure on the level below (sect. 4.3).

A preliminary test was conducted in which the model was illuminated by the LDP from every azimuthal angle. The LDP was rotated 360 deg around the model while a 3-m slant range to TP1 was maintained. The elevation of the LDP was constant at 0.52 m, and the angle (θ) did not change from 10 deg. The rotation device was stopped at 15 deg increments and the current induced at TP1 by the LDP was observed and/or recorded. This exercise showed that the model responded symmetrically to the azimuthal variation of the radiating source, since the induced

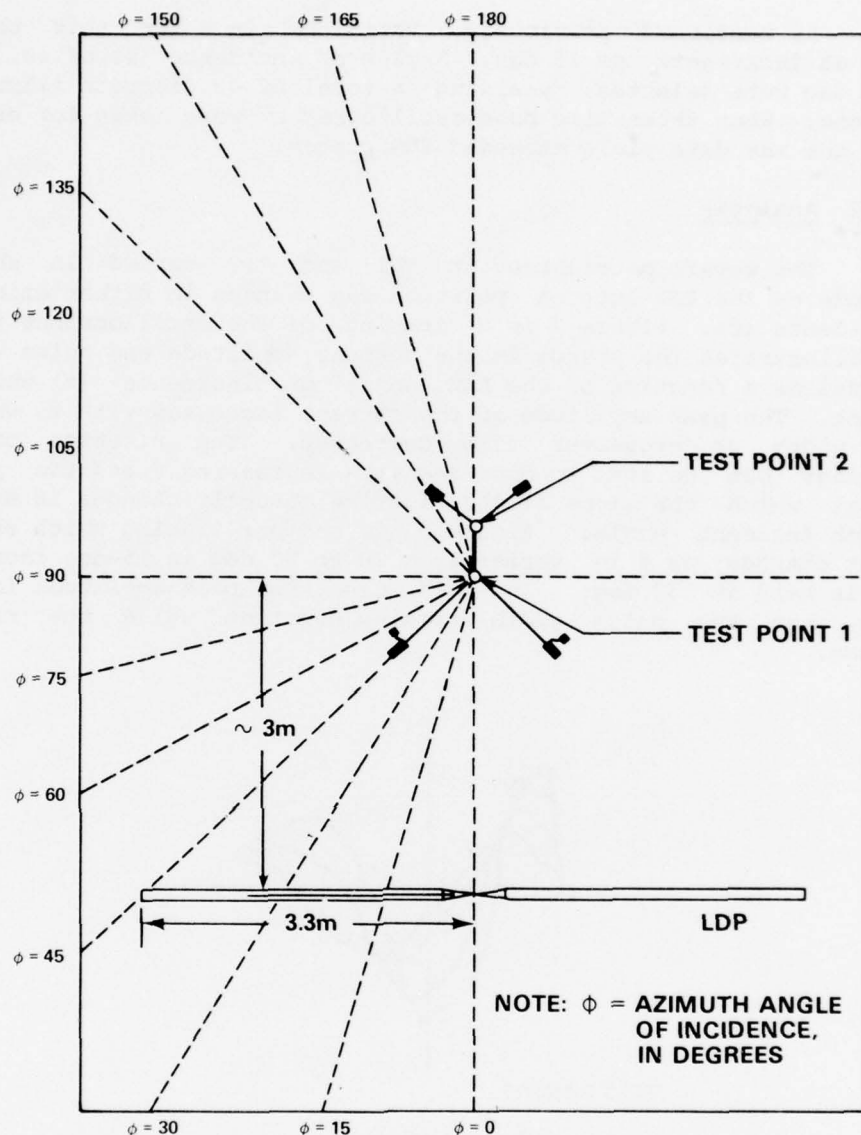


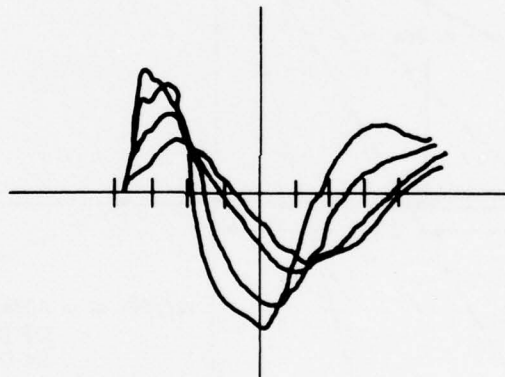
Figure 6. Azimuthal layout of BSC and illuminator.

currents from one side to the other were of the same amplitude, but of opposite sign. That is, the observed waveforms such as $\phi = 45$ and 90 deg were identical to those at $\phi = 315$ and 270 deg, but opposite in polarity. This feature assured that all pertinent data could be collected by restricting the azimuthal variations from $\phi = 0$ deg to $\phi = 180$ deg (fig. 6).

As mentioned previously, variations in ϕ for this test were chosen at increments of 15 deg. Angles of incidence (β) of 10, 30, 60, and 90 deg were selected, yielding a total of 48 discrete illumination positions. When three time-base oscillographs were taken for each test point, the raw data yield exceeded 280 pieces.

5.2 Analysis

The waveforms recorded at TP1 and TP2 varied in shape and amplitude as the LDP antenna position was changed in either azimuth (ϕ) or incidence (β). Figure 7 is a tracing of the oscillographs from TP1 which illustrates the change in the current amplitude and pulse width of the model as a function of the LDP angle of incidence (β) while ϕ is constant. The peak amplitude of the current increases with β , while the pulse width or crossover time decreases. The risetime of these recordings can be seen to decrease with increasing β and the point in time at which the slope of the risetime abruptly changes is different for each incident angle. Figure 8 is another tracing which shows TP1 current changes as ϕ is varied from 30 to 90 deg in 15-deg increments, and β is held at 30 deg. In this case, the peak amplitude increases with ϕ , but the pulse width remains constant while the risetimes decrease.



TEST POINT 1

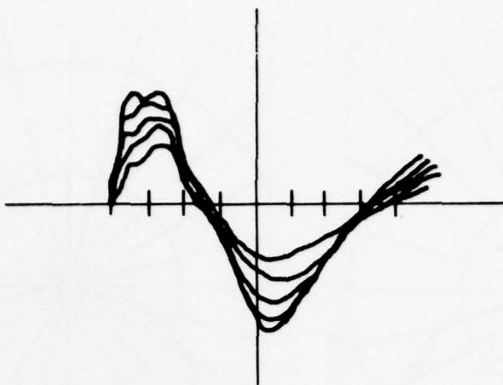
MAINTAIN $\angle \phi = 45 \text{ DEG}$

CHANGE $\angle \beta$ (10, 30, 60, AND 90 DEG)

50 mV/DIV

5 ns/DIV

Figure 7. Waveforms as function of angle of incidence. (Note: peak current amplitude increases with increase in β .)



TEST POINT 1

MAINTAIN $\angle\beta = 30$ DEG

CHANGE $\angle\phi$ (30, 45, 60, 75, AND 90 DEG)

50 mV/DIV

5 ns/DIV

Figure 8. Waveforms as function of azimuth angle. (Note: peak current amplitude increases with increase in ϕ .)

The BSC peak-current variations at TP1 and TP2 for changes in ϕ at all four incident angles (β) are plotted in polar form in figure 9. The amplitudes plotted are in table I. The peak is defined as the greatest level attained by the waveform before the first crossover. While the plots are from 0 to 180 deg, it is understood that 180 to 360 deg would be a mirror image if plotted. Since the waveforms in most cases show a clearly definable point where the slope of the risetime abruptly changes, the amplitudes of the waveforms at these points were also plotted in figure 10. Table II lists the amplitudes of these points.

The peak amplitude graphs* show clearly that the maximum coupling from LDP to model occurs under broadside ($\phi = 90$ deg) illumination. While there is a slight angular shifting of the plotted lobes as the LDP height (and thus β) was changed, it can be seen that the maxima occurred between 75 and 105 deg (ϕ). These graphs are useful in observing the effect of β on the coupling. They show that both the magnitude and beamwidth of the coupling lobes are increasing with β . The beamwidth of these lobes is defined as the angular width measured between two points where the amplitude is 0.5 (-6 dB) of that in the maximum direction. This analysis shows that the peak waveform beamwidths are as follows.

*These graphs show amplitudes plotted every 15 deg, but the waveforms at both test points were observed continuously as the LDP was rotated from point to point. The plotted points are joined to more clearly demonstrate the model's coupling "lobes."

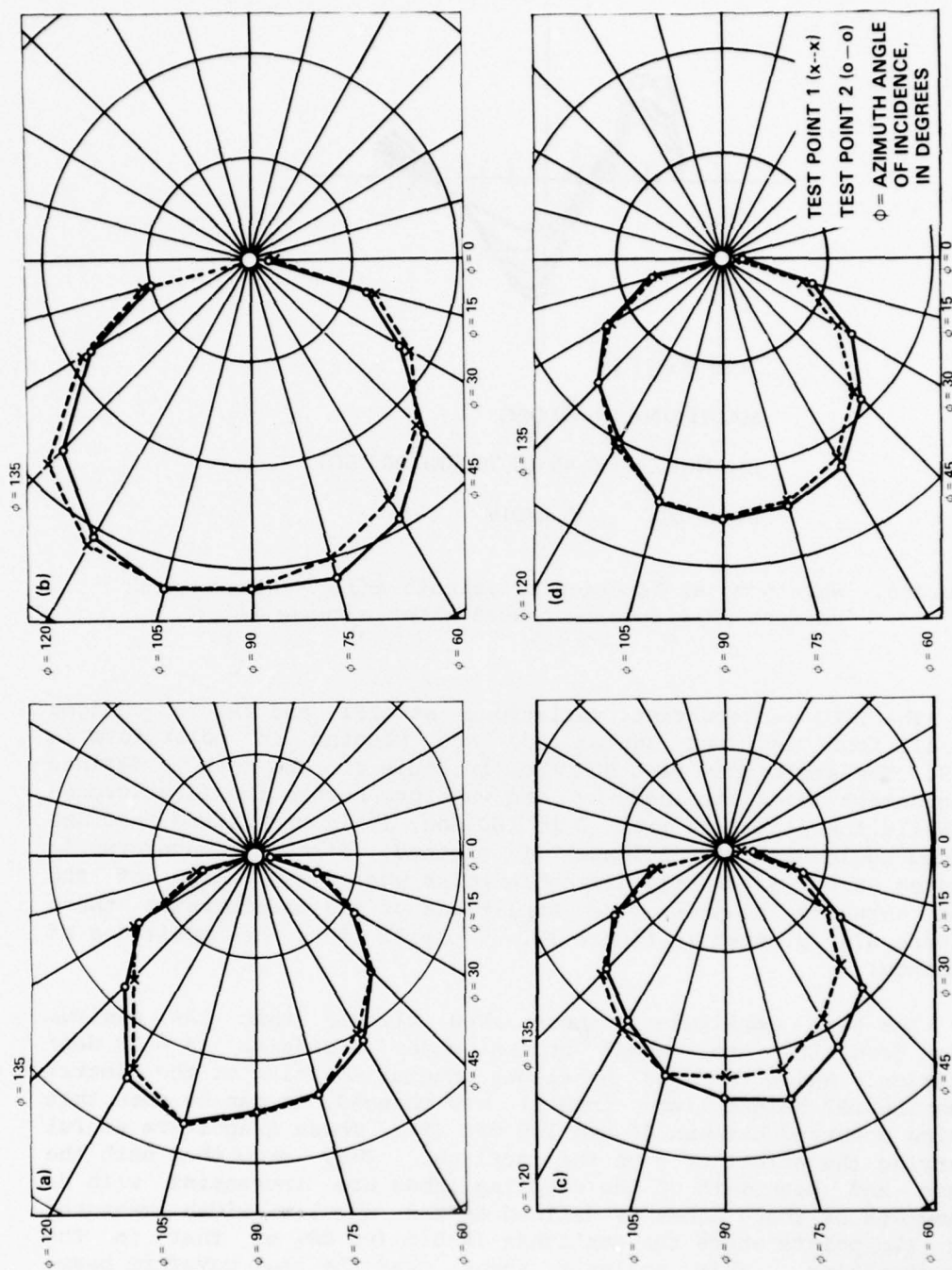


Figure 9. Absolute peak amplitude versus azimuth angle, (a) angle of incidence $\beta = 10$ deg, (b) angle of incidence $\beta = 30$ deg, (c) angle of incidence $\beta = 60$ deg, (d) angle of incidence $\beta = 90$ deg. Note: See table I for amplitude scale factors.

TABLE 1. PEAK CURRENT VALUES AS FUNCTION OF AZIMUTH ANGLE FOR CONSTANT ANGLE OF INCIDENCE.

Azimuth angle ϕ (deg)	Angle of incidence β											
	$\beta = 10$ deg				$\beta = 30$ deg				$\beta = 60$ deg			
	TP1 (mV)	TP1 (mA) \pm	TP2 (mV)	TP2 (mA) \pm	TP1 (mV)	TP1 (mA) \pm	TP2 (mV)	TP2 (mA) \pm	TP1 (mV)	TP1 (mA) \pm	TP2 (mV)	TP2 (mA) \pm
0	8	1.6	8	1.6	12	2.4	9	1.8	15	3	18	3.6
15	32	6.4	32	6.4	64	12.8	58	11.6	68	13.6	76	15.2
30	56	11.2	56	11.2	90	18	85	17	115	23	130	2.6
45	80	16	80	16	115	23	120	24	160	32	185	37
60	100	20	105	21	135	27	145	29	190	38	220	44
75	120	24	120	24	150	30	160	32	220	44	250	50
90	125	25	125	25	160	32	160	32	220	44	240	48
105	135	27	135	27	165	33	165	33	230	46	225	45
120	120	24	125	25	160	32	155	31	200	40	190	38
135	85	17	90	18	140	28	130	26	170	34	165	33
150	68	13.6	65	13	95	19	90	18	120	24	125	25
165	30	6	27	5.4	54	10.8	50	10	70	14	70	14
180	-14	-2.8	-11	-2.2	-7	-1.4	4	0.8	-10	-2	-7	-1.4
270	-125	-25	-120	-24	-160	-32	-	-	-	-	-	-

*Transfer function of Tektronix CT-1 is 5 mV/mA.

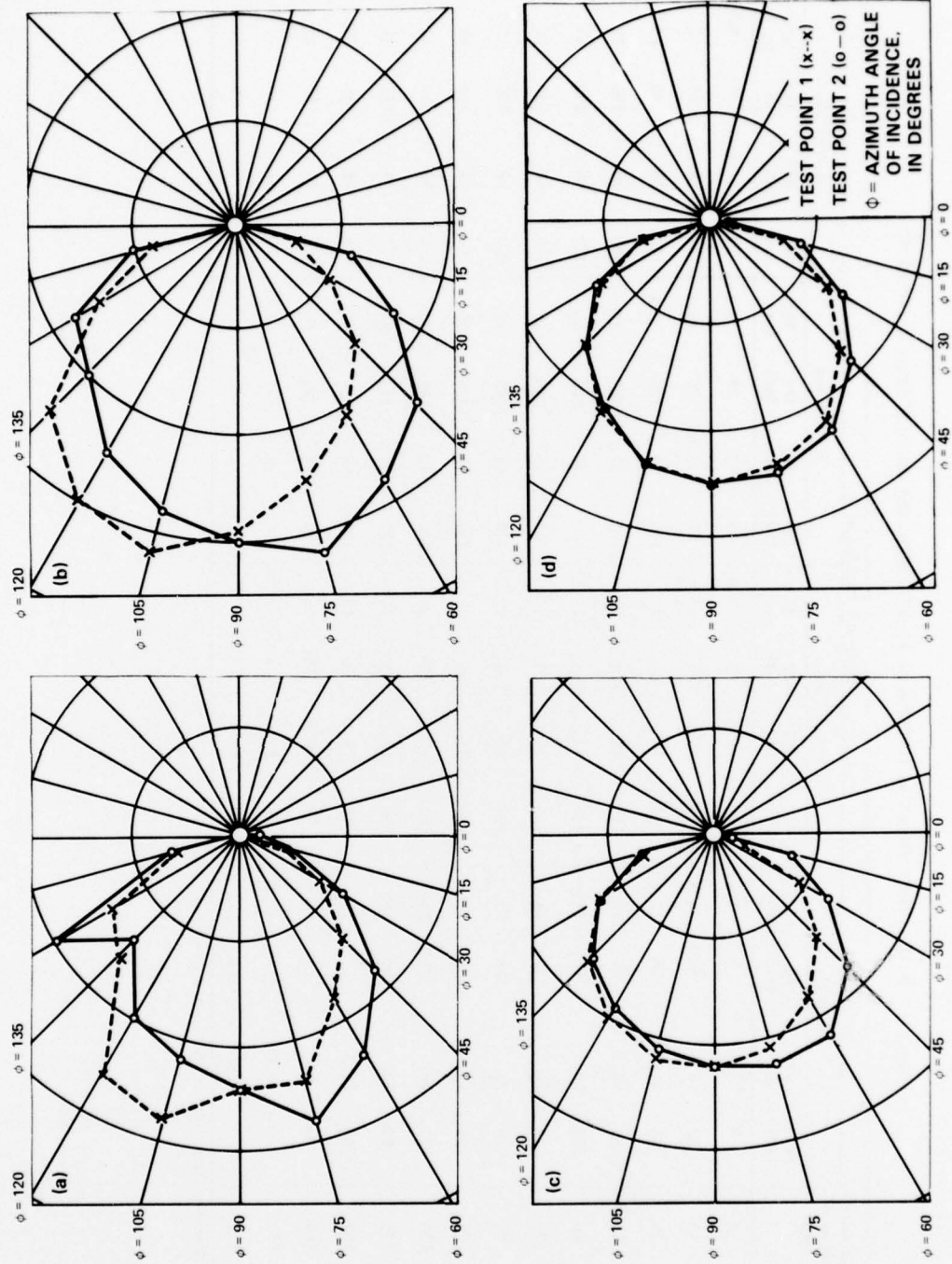


Figure 10. First peak amplitude versus azimuth angle, (a) angle of incidence $\beta = 10$ deg, (b) angle of incidence $\beta = 30$ deg, (c) angle of incidence $\beta = 60$ deg, (d) angle of incidence $\beta = 90$ deg. Note: See table II for amplitude scale factors.

TABLE II. SLOPE CHANGE AMPLITUDE POINT

Azimuth angle ϕ (deg)	Constant angle of incidence β																			
	$\beta = 10 \text{ deg}$				$\beta = 30 \text{ deg}$				$\beta = 60 \text{ deg}$				$\beta = 90 \text{ deg}$							
	TP1 (mV)	TP1 (mA) **	TP2 (mV)	TP2 (mA) **	TP1 (mV)	TP1 (mA) **	TP2 (mV)	TP2 (mA) **	TP1 (mV)	TP1 (mA) **	TP2 (mV)	TP2 (mA) **	TP1 (mV)	TP1 (mA) **	TP2 (mV)	TP2 (mA) **	TP1 (mV)	TP1 (mA) **	TP2 (mV)	TP2 (mA) **
0	6	1.2	5	1	5	1	8	1.6	7	1.4	17	3.4	9	1.8	17	3.4				
15	10	2	15	3	36	7.2	56	11.2	30	6	76	15.2	75	15	90	18				
30	22	4.4	28	5.6	52	10.4	85	17	90	18	125	25	130	26	145	29				
45	35	7	45	9	80	16	120	24	140	28	180	36	175	35	190	38				
60	45	9	60	12	105	21	145	29	180	36	220	44	220	44	230	46				
75	60	12	70	14	125	25	160	32	210	42	225	45	240	48	245	49				
90	60	12	60	12	145	29	150	30	220	44	220	44	250	50	250	50				
105	70	14	55	11	160	32	140	28	220	44	210	42	240	48	240	48				
120	65	13	50	10	150	30	125	25	200	40	190	38	210	42	205	41				
135	40	8	70	14	125	24	100	20	170	34	165	33	170	34	170	34				
150	35	7	50	10	75	15	90	18	125	25	125	25	120	24	125	25				
165	15	3	17	3.4	40	8	50	10	65	13	70	14	60	12	66	13.2				
180	-2	-0.4	-5	-1	-2	-0.4	2	0.4	-10	-2	-6	-1.2	-8	-1.6	-12	2.4				
270	-65	-13	-70	-14	-160	-32	-165	-33	-	-	-	-	-	-	-	-				

*Transfer function of Tektronix CT-1 is 5 mV/mA.

β (deg)	Beamwidth (deg)
10	110
30	123
60	127
90	127

The amplitudes of the points at which the leading edge of the waveforms abruptly changes slope are plotted in figure 10. The graphs for $\beta = 60$ and 90 deg are practically the same as those of the peak amplitude plots at the same elevation angles, since there was almost no slope change to the risetimes of these waveforms. The $\beta = 30$ -deg graph (fig. 10b) shows approximately the same amplitude as the corresponding "peak" graph (fig. 9b), but there is a separation in the lobe patterns of TP1 and TP2. That is, the plot of TP1 current response shows a maximum at 105 deg (ϕ), while the TP2 maximum is at 75 deg (ϕ). The $\beta = 10$ -deg graph (fig. 10a) also shows this test-point lobe separation plus a quirk in both patterns from 135 to 150 deg, ϕ . These quirks may be due to the end firing of the short wire (0.51 m) which ran from TP2 toward one of the jeep vehicles. For purposes of symmetry, this wire was laid out so that it pointed at $\phi = 135$ deg for the test volume, while the other short wire from the TP2 junction pointed toward 225 deg. When the LDP was positioned at $\phi = 135$ deg, it was approximately end firing the wire at this angle, since the axis of rotation was at TP1, not TP2. However, this was the position in which the 135 -deg wire was as close as it came to being parallel to the center line, or equatorial plane, of the LDP. It is of interest to note that this anomaly is present only at the lowest elevation angle ($\beta = 10$ deg) and only observable in the examination of the early portion of the risetime, that is, the point at which the leading edge abruptly changes slope. In fact, this particular plotted function (fig. 10a) is the only one that differs markedly in amplitude and shape from the corresponding graph of peak amplitude.

The induced-current responses recorded from the BSC in this scale-model test clearly demonstrate the effects of azimuthal and incident angle of the EMP simulation. Figures 11 and 12 plot the induced current at model TP1 versus ϕ , the azimuth angle. Four angles of incidence are plotted, all of which have been normalized to the model's maximum current response. The plotted data are given in tables III and IV.

Figure 11 shows the absolute peak, that is, the greatest level attained by the current waveforms. Figure 12 shows the first peak, that amplitude on the risetime of the current waveforms at which there is a noticeable abrupt change in the slope. Again, as in a comparison of the

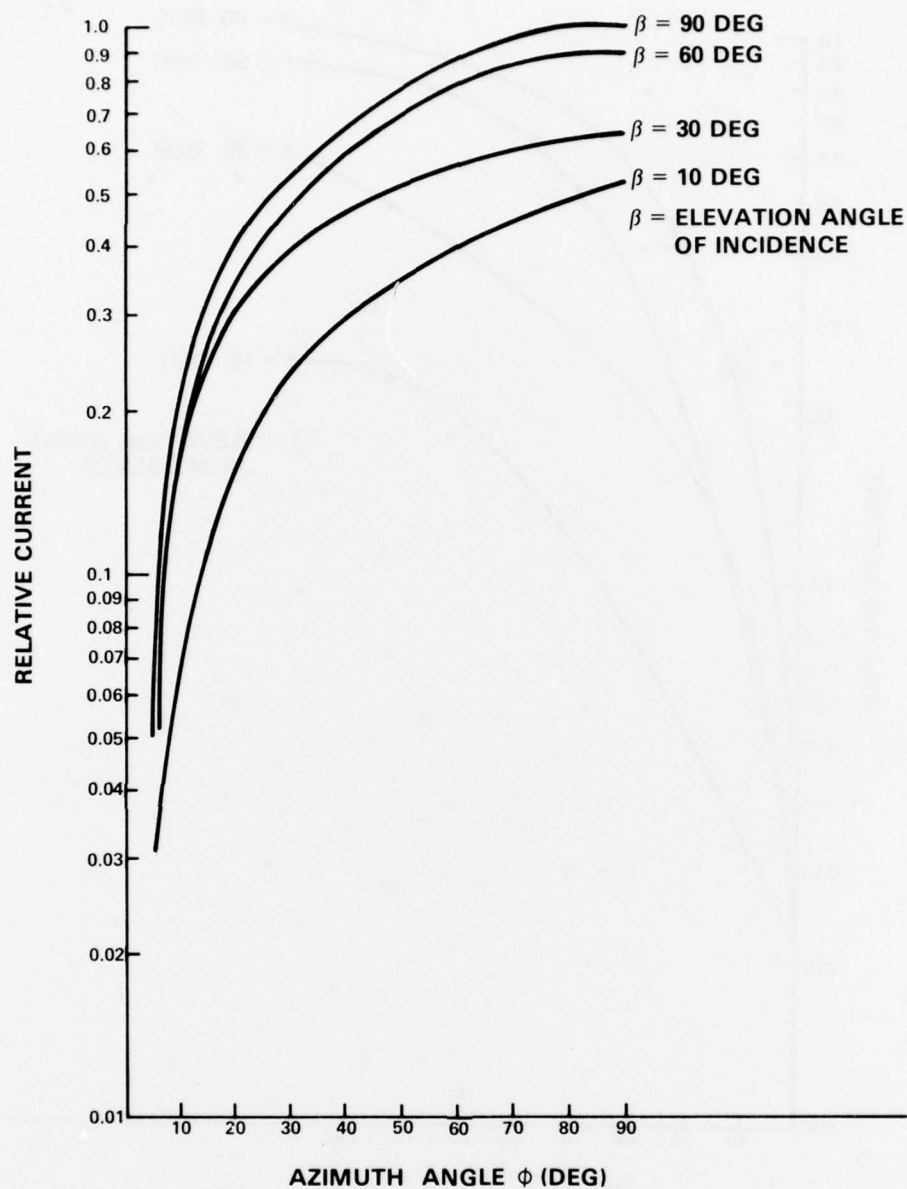


Figure 11. Absolute peak plot.

previous polar plots of these currents, it can be seen that when $\beta = 10$ deg the first peak and absolute peak differ markedly. In fact, if the worst-case illumination for the BSC is considered ($\phi = 90$ deg), the angle of incidence variation from 10 to 90 deg causes an increase of a

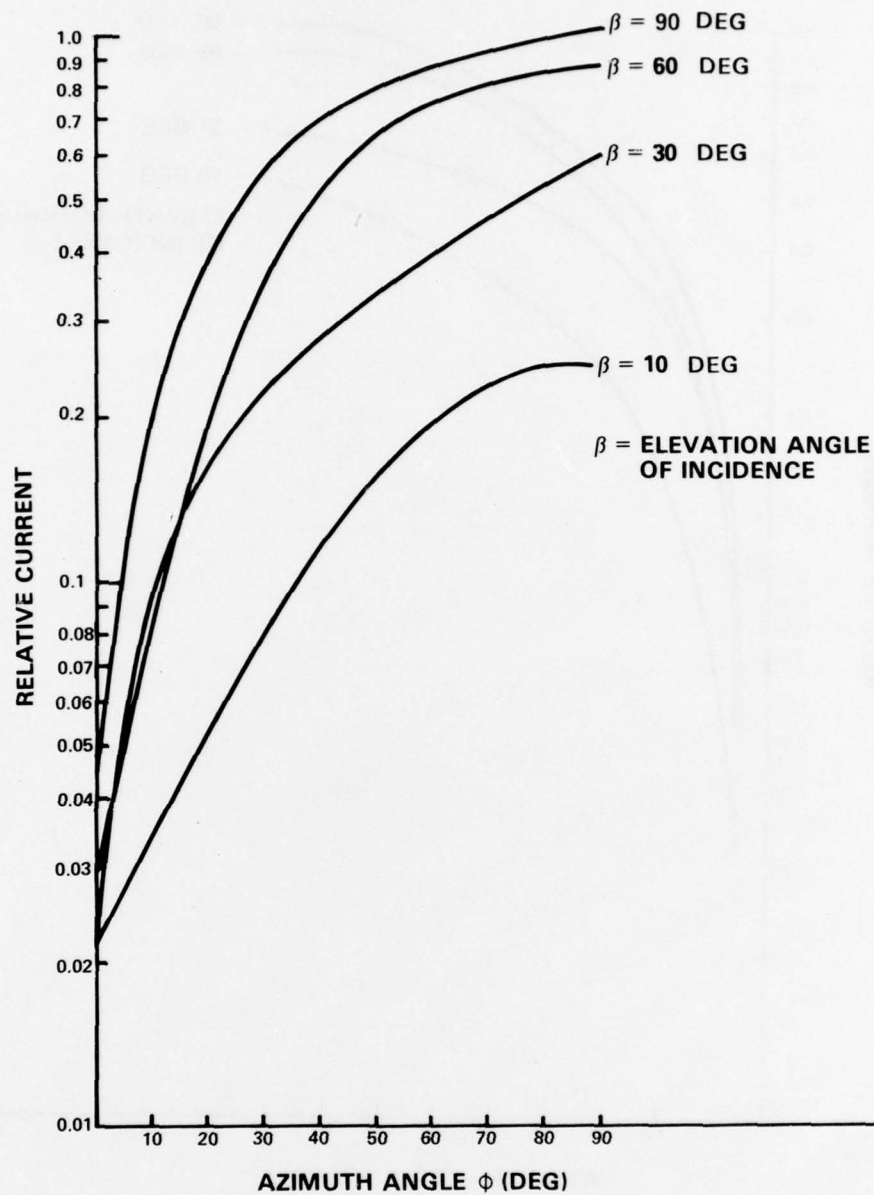


Figure 12. First peak plot.

factor of four in the value of the first peak current (fig. 12), whereas the absolute peak increases by only a factor of two (fig. 11). A positive statement on the double peaks is difficult based just on the modeling results, but reference to figure 13 is interesting. In this

TABLE III. ABSOLUTE PEAK VALUE NORMALIZED TO $\beta = 90$ deg,
 $\phi = 90$ deg (250 mV)

ϕ (deg)	$\beta = 10$ deg		$\beta = 30$ deg		$\beta = 60$ deg		$\beta = 90$ deg	
	TP1	TP2	TP1	TP2	TP1	TP2	TP1	TP2
90	0.50	0.50	0.64	0.64	0.88	0.96	1.0	1.0
75	0.48	0.48	0.60	0.64	0.88	1.0	0.96	1.0
60	0.40	0.42	0.54	0.58	0.76	0.88	0.88	0.92
45	0.32	0.32	0.46	0.48	0.64	0.74	0.72	0.78
30	0.22	0.22	0.36	0.34	0.46	0.52	0.52	0.56
15	0.13	0.13	0.26	0.23	0.27	0.30	0.32	0.34
0	0.03	0.03	0.05	0.04	0.06	0.07	0.05	0.07

TABLE IV. FIRST PEAK (SLOPE CHANGE) VALUE NORMALIZED TO $\beta = 90$ deg,
 $\phi = 90$ deg (250 mV)

ϕ (deg)	$\beta = 10$ deg		$\beta = 30$ deg		$\beta = 60$ deg		$\beta = 90$ deg	
	TP1	TP2	TP1	TP2	TP1	TP2	TP1	TP2
90	0.24	0.24	0.58	0.60	0.88	0.88	1.0	1.0
75	0.24	0.28	0.50	0.64	0.84	0.90	0.96	0.98
60	0.18	0.24	0.42	0.58	0.72	0.88	0.88	0.92
45	0.14	0.18	0.32	0.48	0.56	0.72	0.70	0.76
30	0.09	0.11	0.21	0.34	0.36	0.5	0.52	0.58
15	0.04	0.06	0.14	0.22	0.12	0.30	0.30	0.36
0	0.02	0.02	0.02	0.03	0.03	0.07	0.04	0.07

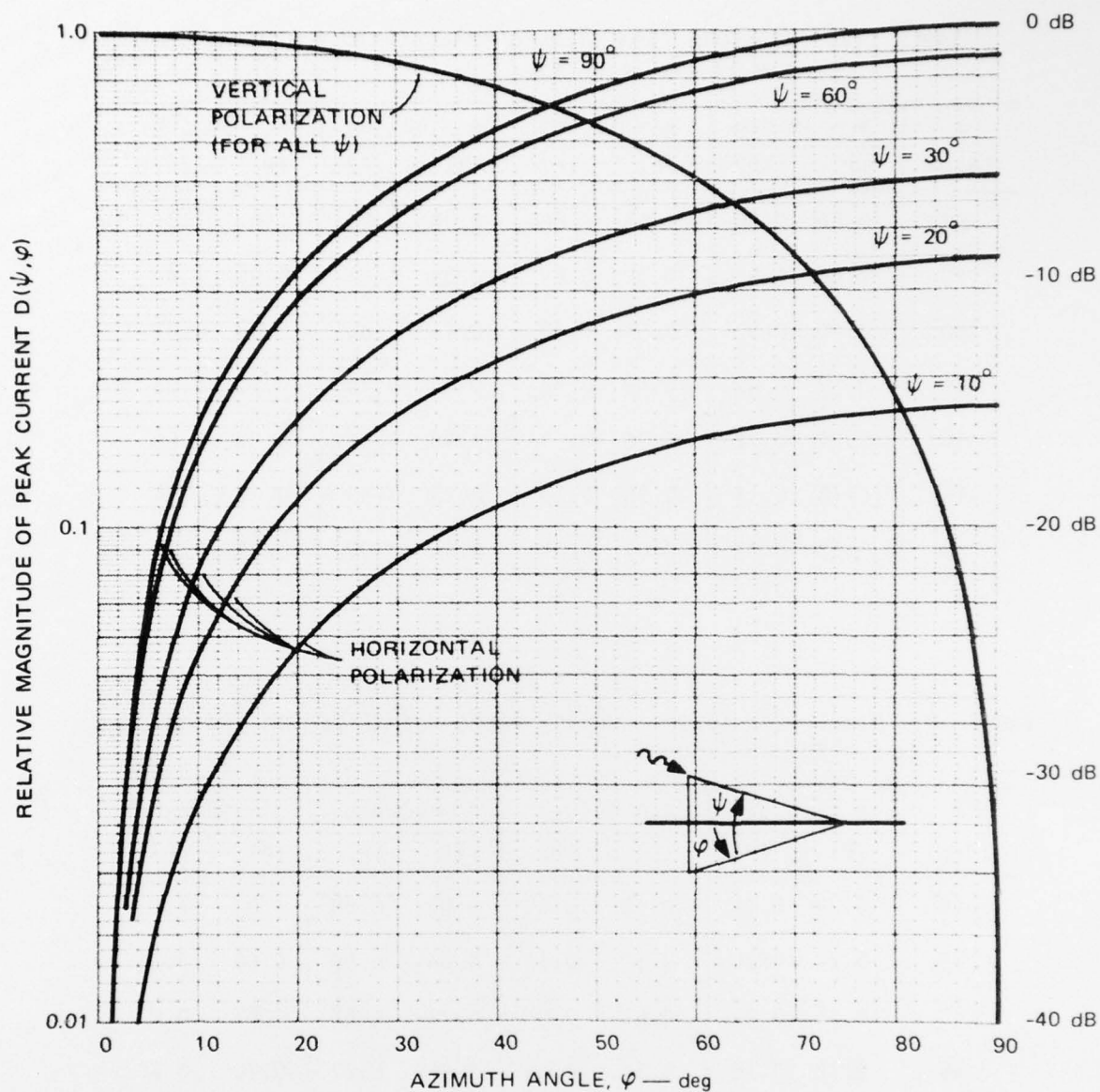


Figure 13. Variation of peak cable current as azimuth (ϕ) and elevation (ψ) angles of incidence change (reproduced from Vance, 1973)
Note: $\psi \approx \beta$

graph, Vance⁷ shows the calculated-response characteristics of a point on a cable (buried near the surface) far from the end as the azimuth and elevation angles are varied. The variation between a 10- and 90-deg elevation angle (azimuth = 90 deg), in this case, causes an increase in current of a factor of 5.76, as the response changes with the sine of the angle of incidence. In comparison, the first-peak graph therefore more closely follows what, in general, the theory would dictate for a long cable buried near the surface of the ground.

Gray* has noticed the second peak in calculations and full-scale measurements which he has made. He concludes that it is a function of cable configuration and terminating impedances as well as the shape of the incident field which is affected by the nearness of the radiating antenna to the ground.

6. CONCLUSIONS

The results of this experiment yield practical data of interest to those involved in real-world EMP testing. For broadside illumination, the cable connected to the AN/TRC-145 switchboard and the TCC-29 switchboard would experience a factor of four** increase in induced bulk current if it were possible to increase the angle of incidence from 10 to 90 deg. No significant contributions to this current are made by the model's radial arms from the switchboard to the two AN/TRC-145's and from the TCC-29 to the jeeps. Apparently, currents induced in these arms do vary with azimuth, but the grounds of the model prevented the monitored points from varying except as a single wire would.

Further study is necessary to ascertain the true nature of the lower elevation response waveforms.

In other experimental work, we have observed that a long wire shows a response similar to that of the BSC observed here. Further, the unusual second peak was more predominant at low angles of incidence and present even when two different illuminating sources were used. As the wire was moved away from the radiator maintaining a constant angle of incidence, we observed that while the first peak falls off as $1/r$ (where r is the radial distance from the source), the second or absolute peak varies as $r^{-1.83}$.

⁷E. F. Vance, *Predictions of Transients in Buried Shielded Cables*, Stanford Research Institute (March 1973).

*R. Gray, HDL, private communication.

**Using the first peak plot.

LITERATURE CITED

- (1) U.S. Army FM 11-125, Field Army Signal Communications, Headquarters Dept. Army (December 1969).
- (2) U.S. Army FM 24-16, Signal Orders Records and Reports, Headquarters Dept. Army (May 1970).
- (3) U.S. Army FM 24-18, Field Radio Techniques, Headquarters Dept Army (July 1965).
- (4) G. Sinclair, Theory of Models of Electromagnetic Systems, Proc. Institute of Radio Engineers (November 1948), 1364-1370.
- (5) J. Kreck, Electromagnetic Scale Model of TEMPS/Polk City Test Configuration, Harry Diamond Laboratories TR-1717 (March 1976).
- (6) A. Cuneo and J. Loftus, Scale Modeling for the PAR EMP Test, Harry Diamond Laboratories TR-1761 (September 1976).
- (7) E. F. Vance, Predictions of Transients in Buried Shielded Cables, Stanford Research Institute (March 1973).

APPENDIX A.--ADDITIONAL BSC INFORMATION

For the interested reader, an inventory of the brigade signal center (BSC) is included here along with typical equipment placement, interconnection, and grounding.

A-1. VEHICLES AND ASSOCIATED EQUIPMENT

- a. AN/TRC-145, 1-1/4-ton truck with S280/G van.
 - (1) Two AN/GRC-103 radio sets.
 - (2) One dual 12-channel radio terminal set.
 - (3) Two TD660 multiplexers.
 - (4) Two TD754 cable combiners.
 - (5) Two CV1548 converters.
 - (6) Two KG27 key generators.
- b. TCC-29--switchboard vehicular transportable for nonsecure facilities (60 lines); also has facilities for connecting 26 pairs of cables; operates on its own portable power supply.
- c. SSB-22/PT switchboard (portable); weighs 13.6 kg, is operated on flashlight batteries. The SSB-22/PT is located in a tent, connected to the TCC-29 switchboard; also connected to two or more vehicles. These vehicles are normally jeeps which use FM and wire communications. The equipment is generally the VRC-46 or VRC-47.

A-2. VEHICLE AND EQUIPMENT PLACEMENT

- a. AN/TRC-145 Multiplex (MUX) Vans and Antennas should be on the edge of the site nearest the site to which the antennas are transmitting.
- b. Radio and Teletype rigs (RATT) should be on the opposite side of site with relation to the AN/TRC-145 MUX vans.
- c. Power units should be placed as far as possible from antenna and radio terminal sets to minimize interference (a minimum of 15 m).

APPENDIX A

d. All vehicles should be at least 60 m apart.

e. All shelters and power-generating equipment should be thoroughly grounded before placing them in operation. All vehicles and trailers with radio or generator equipment should be grounded. Ground rods should be at least 1.5 m long.

f. The interconnection between a radio set at a radio-wire integration station and an area communications-system switchboard should be made through an AN/GSA-7 radio control set with a 5- to 10-pin adapter cable CX-7474/U and an SSB-22/PT switchboard. By using the AN/GSA-7, the distance between radio and telephone equipment has been extended from 3.2 to 16 km.

For planning purposes, the range of field-wire circuits using battery-operated telephones is from 22 to 35 km. With sound-powered telephones, the range is 5 to 16 km.

Note: All vans have Cannon plugs at cable entries. The MUX van cable entry is at the rear of the van. Switchboard cable connection is on the side.

DISTRIBUTION

DEFENSE DOCUMENTATION CENTER
CAMERON STATION, BUILDING 5
ALEXANDRIA, VA 22314
ATTN DDC-TCA (12 COPIES)

COMMANDER
USA RSCH & STD GP (EUR)
BOX 65
FPO NEW YORK 09510
ATTN LTC JAMES M. KENNEDY, JR.
CHIEF, PHYSICS & MATH BRANCH

COMMANDER
US ARMY MATERIEL DEVELOPMENT
& READINESS COMMAND
5001 EISENHOWER AVENUE
ALEXANDRIA, VA 22333
ATTN DRXAM-TL, HQ TECH LIBRARY

COMMANDER
US ARMY ARMAMENT MATERIEL
READINESS COMMAND
ROCK ISLAND ARSENAL
ROCK ISLAND, IL 61201
ATTN DRSAR-ASF, FUZE & MUNITIONS SPT DIV

COMMANDER
USA MISSILE & MUNITIONS CENTER & SCHOOL
REDSTONE ARSENAL, AL 35809
ATTN ATSK-CTD-F

DIRECTOR
DEFENSE ADVANCED RESEARCH
PROJECTS AGENCY
ARCHITECT BLDG
1400 WILSON BLVD
ARLINGTON, VA 22209
ATTN DIR, NUCLEAR MONITORING RES OFFICE

DEFENSE COMMUNICATION ENGINEERING CENTER
1860 WIEHLE AVE
RESTON, VA 22090
ATTN TECHNICAL LIBRARY

DIRECTOR
DEFENSE COMMUNICATIONS AGENCY
DEPT OF DEFENSE
WASHINGTON, DC 20305
ATTN TECH LIBRARY

DIRECTOR
DEFENSE COMMUNICATIONS AGENCY
NATIONAL MILITARY COMMAND
SYSTEM SUPPORT CENTER
WASHINGTON, DC 20301
ATTN TECHNICAL DIRECTOR (B102)

DIRECTOR
DEFENSE NUCLEAR AGENCY
WASHINGTON, DC 20305
ATTN ELECTRONIC VULNERABILITY DIV (RAEV)
ATTN TECHNICAL LIBRARY (APTL)
ATTN INFORMATION SYSTEMS DIV (VLIS)

DIRECTOR OF DEFENSE RESEARCH & ENGINEERING
WASHINGTON, DC 20301
ATTN ASST DIR (ELECTRONICS &
PHYSICAL SCIENCES)
ATTN ASST DIR (ENG TECHNOLOGY)
ATTN DEP DIR (STRATEGIC & SPACE SYS)

COMMANDER
FIELD COMMAND
DEFENSE NUCLEAR AGENCY
KIRTLAND AFB, NM 87115
ATTN FCSD-A4, TECH REF BR

DIRECTOR
NATIONAL SECURITY AGENCY
FORT GEORGE G. MEADE, MD 20755
ATTN TECHNICAL LIBRARY

OFFICE, DEPUTY CHIEF OF STAFF FOR
OPERATIONS & PLANS
DEPT OF THE ARMY
WASHINGTON, DC 20310
ATTN DAMO-SSA, NUCLEAR/CHEMICAL
PLANS & POLICY DIV

BALLISTIC MISSILE DEFENSE PROGRAM
MANAGER OFFICE
COMMONWEALTH BUILDING
1300 WILSON BLVD
ARLINGTON, VA 22209
ATTN DACS-BMS, ASST FOR SAFEGUARD

COMMANDER
BALLISTIC MISSILE DEFENSE SYSTEMS COMMAND
PO BOX 1500
HUNTSVILLE, AL 35807
ATTN BMDSC-W, SAFEGUARD PROJECT OFFICE
ATTN TECH LIB

COMMANDER
BALLISTIC MISSILE DEFENSE ADVANCED
TECHNOLOGY CENTER
PO BOX 1500
HUNTSVILLE, AL 35807
ATTN TECH LIB

COMMANDER
US ARMY COMMUNICATIONS COMMAND
FORT HUACHUCA, AZ 85613
ATTN TECH LIB

CHIEF
US ARMY COMMUNICATIONS SYS AGENCY
FORT MONMOUTH, NJ 07703
ATTN SCCM-AD-SV, LIBRARY

COMMANDER
US ARMY NUCLEAR AGENCY
BUILDING 2073
7500 BACKLICK ROAD
SPRINGFIELD, VA 22150
ATTN TECH LIB

DISTRIBUTION (Cont'd)

COMMANDER
US ARMY SAFEGUARD COMMUNICATIONS AGENCY
FORT HUACHUCA, AZ 85613
ATTN SCCX-SSA, SPECIAL SCIENTIFIC
ACTIVITIES DIR

COMMANDER
CORPS OF ENGINEERS
HUNTSVILLE DIVISION
PO BOX 1600
HUNTSVILLE, AL 35807
ATTN T. BOLT (3 COPIES)

COMMANDER
NAVAL SURFACE WEAPONS CENTER
WHITE OAK, MD 20910
ATTN WA-50, NUCLEAR WEAPONS
EFFECTS DIV

COMMANDER
AF WEAPONS LAB, AFSC
KIRTLAND AFB, NM 87117
ATTN SE, NUCLEAR SYS DIV
ATTN EL, ELECTRONICS DIV

UNIVERSITY OF CALIFORNIA
LAWRENCE LIVERMORE LABORATORY
PO BOX 808
LIVERMORE, CA 94550
ATTN E. K. MILLER

ITT RESEARCH INSTITUTE
10 WEST 35TH STREET
CHICAGO, IL 60616
ATTN I. N. MINDEL
ATTN J. E. BRIDGES

KAMAN SCIENCES CORP
PO BOX 7463
COLORADO SPRINGS, CO 80933
ATTN DR. HOFFMAN

STANFORD RESEARCH INSTITUTE
3980 EL CAMINO REAL
PALO ALTO, CA 94306
ATTN A. L. WHITSON

HARRY DIAMOND LABORATORIES
ATTN RAMSDEN, JOHN J., COL, COMMANDER/
FLYER, I.N./LANDIS, P.E./
SOMMER, H./OSWALD, R. B.
ATTN CARTER, W.W., DR., TECHNICAL
DIRECTOR/MARCUS, S.M.
ATTN WISEMAN, ROBERT S., DR., DRDEL-CT
ATTN KIMMEL, S., PAO
ATTN CHIEF, 0021
ATTN CHIEF, 0022
ATTN CHIEF, LAB 100
ATTN CHIEF, LAB 200
ATTN CHIEF, LAB 300
ATTN CHIEF, LAB 400
ATTN CHIEF, LAB 500
ATTN CHIEF, LAB 600
ATTN CHIEF, DIV 700
ATTN CHIEF, DIV 800
ATTN CHIEF, LAB 900
ATTN CHIEF, LAB 1000
ATTN RECORD COPY, BR 041
ATTN HDL LIBRARY (5 COPIES)
ATTN CHAIRMAN, EDITORIAL COMMITTEE
ATTN CHIEF, 047
ATTN TECH REPORTS, 013
ATTN PATENT LAW BRANCH, 071
ATTN GIDEP OFFICE, 741
ATTN LANHAM, C., 0021
ATTN DYCKSON, R. A., 1040
ATTN LOFTUS, J. J., 1040
ATTN CUNEO, A. A., 1040 (30 COPIES)
ATTN DANDO, J. D., 1040